ELSEVIER

View angle effects on relationships between MISR vegetation indices and leaf area index in a recently burned ponderosa pine forest

Amy Pocewicz [a],*, Lee A. Vierling [a], Leigh B. Lentile [a], Rachel Smith [b]

[a] College of Natural Resources, University of Idaho, Moscow, ID 83844, United States
[b] College of Forestry and Conservation, University of Montana, Missoula, MT 59812, United States

Abstract

While nadir-viewing passive multispectral sensors have limited utility for characterizing the full dimensionality of forest canopies, multi-angle remote sensors such as the Multi-angle Imaging SpectroRadiometer (MISR) may improve detection of canopy architecture, canopy cover, and leaf area index (LAI) of forest canopy versus understory vegetation. Our objective was to determine whether data from the MISR sensor could improve estimates of LAI across a post-fire ponderosa pine forest located in the Black Hills of South Dakota. We measured LAI during the 2002 and 2003 growing seasons and created continuous LAI maps using Landsat TM and ETM+ data (mean $R^2 = 0.81$). We fit linear regression models of total and canopy LAI, using a series of MISR at-nadir and off-nadir or anisotropic vegetation indices as predictor variables, for each of five sampling periods. We found the best LAI model fits using either a new hotspot-adjusted normalized difference vegetation index, $NDVI_{HS}$, NDVI calculated from the $-60°$ view angle, or NDVI at-nadir and either the Hotspot–DarkSpot Index (HDS) or the normalized difference anisotrophic index (NDAX) ($R^2 = 0.56–0.91$). However, differences in fits of these best models and those including NDVI at-nadir ranged from only 1 to 8%. Reflectance anisotropy patterns related strongly to understory vegetation phenology. We found that the relationships among NDVI or the enhanced vegetation index (EVI) and canopy or total LAI showed little variation across view angles when the understory vegetation was senesced and significant anisotropy when understory green LAI was greatest. These findings demonstrate the value of multi-temporal measurements during periods of understory phenological change, even if the overstory LAI is relatively stable. We also evaluated the performance of the MISR LAI product and found moderate fits between the MISR LAI and our field- and Landsat-derived canopy LAI ($R^2 = 0.21–0.44$).
© 2006 Elsevier Inc. All rights reserved.

Keywords: MISR; Landsat; Multi-angle remote sensing; LAI; NDVI; EVI; RSR; *Pinus ponderosa*; Mixed-effects models; Theil–Sen regression; Disturbance

1. Introduction

Forest canopy structure significantly affects ecosystem function by influencing light attenuation and water, trace gas, and nutrient fluxes. As a result, there is a great need to map changes in canopy structural attributes such as leaf area index (LAI). While nadir-viewing passive multispectral sensors have limited utility for characterizing the full dimensionality of forest canopies, multi-angle remote sensors such as the Multi-angle Imaging SpectroRadiometer (MISR) may improve detection of canopy architecture, canopy cover, and LAI of forest canopy versus understory vegetation (Asner et al., 1998). Indeed, multi-angle remote sensing has recently been used to detect forest canopy structural features including forest cover density and foliage clumping (Chen et al., 2003; Diner et al., 2005; Nolin, 2004; Widlowski et al., 2004). Because strong biochemical and ecological gradients occur vertically within vegetation canopies, extending these multi-angle studies to improve retrievals of LAI may increase our ability to model ecosystem processes across broad spatial extents.

LAI, the projected leaf area per unit ground area, changes seasonally and with disturbances including fires, insect outbreaks, and human management. LAI is directly related to photosynthesis because of its influence on stomatal area and the amount of photosynthetically active radiation absorbed (e.g. Bonan, 1993; Gholz, 1982). It is thus a key state variable in ecosystem process models related to forest productivity, nutrient

---

* Corresponding author.
E-mail address: poce6886@uidaho.edu (A. Pocewicz).

cycling, and water balance (Aber et al., 1996; Waring & Running, 1998; White et al., 2000). Numerous studies have found strong relationships between LAI and remotely sensed reflectance in the red and near-infrared (NIR) wavelengths, due to absorption of radiation in the red wavelengths by chlorophyll pigments and the strong reflectance of NIR wavelengths by leaf mesophyll cells within green vegetation (Gates et al., 1965; Gausman et al., 1973). Vegetation indices that capture this contrast and that are commonly used to predict LAI include the Normalized Difference Vegetation Index (NDVI) (Rouse et al., 1974) and the Simple Ratio (SR) (Birth & McVey, 1968). However, at-nadir, the relationship between LAI and spectral vegetation indices often saturates at intermediate values of LAI. The incorporation of shortwave infrared (SWIR) wavelengths into these vegetation indices reduces the influence of open canopies and soil background (Brown et al., 2000; Nemani et al., 1993) and seems to diminish the vegetation index-LAI saturation problem (Chen et al., 2002; Pocewicz et al., 2004; X. Chen et al., 2005c).

Vegetation indices incorporating multiple view angles have potential to further improve LAI estimation by better accounting for structural variation affecting LAI, such as foliage clumping (Chen et al., 2003) and stand density (Johnson, 1994; Nolin, 2004). The use of multiple view angles may also better distinguish between canopy and understory vegetation due to differences in which vegetation layers can be detected at-nadir and off-nadir view angles and varying degrees of light scattering and shadowing with differing amounts or phenology of understory vegetation (e.g., Vierling et al., 1997). The shapes of angular bidirectional reflectance factor (BRF) signatures have been related to vegetation structure and shadowing within pixels (Nolin, 2004; Pinty et al., 2002; Widlowski et al., 2004), with low to moderate density tree canopies typically exhibiting a bell-shaped angular signature in the red BRF across the solar principal plane (Pinty et al., 2002) and a bowl-shaped pattern in NDVI (Deering et al., 1994, 1999). Differences in angular signature shapes in the red BRF have been found among ponderosa pine (*Pinus ponderosa*) forests differing in density by as little as 13 or 21% (Nolin, 2004). Because stand density is one of the factors influencing LAI, one might also expect to see differences in angular signature shapes associated with different amounts of forest stand LAI. Using data from the POLDER instrument, strong correlations were found between indices quantifying reflectance anisotropy (the Hotspot–DarkSpot (HDS) and Normalized Difference between Hotspot and Darkspot (NDHD) indices) and a foliage clumping index that is an important parameter for LAI calculation in conifer canopies (Chen et al., 2003; Lacaze et al., 2002; J. Chen et al., 2005a). Another anisotropy index, ANIX, was found to be more influenced by forest canopy characteristics than by soil and background effects, which helped to discriminate boreal forest cover types having different canopy shapes (Sandmeier & Deering, 1999a). An anisotropic version of NDVI, the Normalized Difference Anisotropic Index (NADX) calculated from Advanced Solid-State Array Spectroradiometer (ASAS) data, also improved discrimination of these forest cover types, relative to NDVI (Sandmeier & Deering, 1999b). The potential

of these or similar anisotropy indices to improve LAI estimates directly has not yet been evaluated.

Multi-angle remote sensing has already been applied to LAI estimation on a global scale. LAI at 1.1 km spatial resolution is a standard product of the multi-angle MISR sensor (Knyazikhin et al., 1998a). In areas having vegetation cover, MISR data are used to model LAI within each of six biomes: grasses and cereal crops, shrubs, broadleaf crops, savanna, broadleaf forest, and needleleaf (conifer) forest. LAI values are retrieved using canopy models that vary with biome type, canopy structure, and soil/understory reflectance through an algorithm using bihemispherical reflectance (BHR), bidirectional reflectance factor (BRF) and their uncertainties (Hu et al., 2003; Knyazikhin et al., 1998b). The MISR LAI product has been validated across five biomes in Africa (Hu et al., 2003). Although biomes were misclassified in 80% of the pixels, 70% of the time the uncertainties in MISR LAI associated with the misclassification did not exceed uncertainties in the observations (Hu et al., 2003). The MISR LAI product has not been validated within the conifer forest biome, and local studies evaluating its performance are generally lacking. Validation studies do not commonly include areas affected by fire or other natural disturbance regimes; however, fire effects on vegetation may be highly variable, making disturbed landscapes valuable locations for such studies.

Thus, the objectives of our study were to: 1) create and evaluate regional maps of LAI by scaling-up LAI ground measurements via Landsat TM or ETM+ data; 2) determine whether vegetation indices incorporating MISR's multiple view angles improve estimates of conifer forest LAI and whether this varies with changes in canopy and understory LAI over two growing seasons; and 3) compare the MISR LAI product with LAI maps based on ground data across growing seasons in a post-fire landscape. Our study area in the Black Hills of South Dakota is dominated by ponderosa pine forest characterized by low LAI values, allowing us to avoid the saturation of vegetation indices that often occurs with higher LAI values, especially when SWIR data are not available such as in the case of MISR. Ponderosa pine forests range from western California to central Nebraska and from southern British Columbia to northern Mexico (Waring & Law, 2001), and thus our findings may be relevant to large extents of forest across western North America. Our study also evaluates temporal variation in the relationship between LAI and vegetation indices, an important consideration given the fact that LAI changes seasonally and yearly. As in many ponderosa pine forests across the American West, the Black Hills recently experienced a large wildfire with a heterogeneous severity pattern, and LAI changes may be especially pronounced during recovery from such disturbance. We evaluate relationships between MISR data and LAI 2 and 3 years post-fire (2002–2003).

2. Methods

2.1. Study area description

The Black Hills forms the easternmost extension of the Rocky Mountains, rising over 1000 m above the Great Plains in

western South Dakota and northeastern Wyoming. Ponderosa pine is the dominant tree species throughout the Black Hills and is considered the climax species in most locations due to its adaptations to the fire, insect infestations, and drought conditions common to this area. Ponderosa pine vegetation habitat types vary throughout the Black Hills due to local geology and precipitation (Shepperd & Battaglia, 2002).

The area burned by the Jasper Fire is located on the southwestern extent of the fertile Limestone Plateau. In the study area, latitudes range from 43° 41′ 35″ to 43° 55′ 48″ N and longitudes range from 103° 46′ 1″ to 104° 0′ 47″ W. Elevations range from ~ 1500–2100 m. The mean daily maximum and minimum temperatures are −3.3 and 13.2 °C, and annual precipitation ranges from ~ 45 to 48 cm with ~ 75% of precipitation falling in late spring and summer. Forest undergrowth is dominated by graminoids (e.g., *Carex* spp.), several forb species (e.g., *Antennaria* spp. and *Apocynum androsaefolium*), and shrubs (e.g., *Juniperus communis* and *Symphoricarpos* spp.). Pine seed production is high, and natural regeneration is prolific in the study area and throughout the Black Hills (Lentile, 2004).

The Jasper fire, the largest fire in recorded history of the Black Hills of South Dakota, started on August 24, 2000 and was contained 8 days later after burning 33,000 ha of the Black Hills National Forest (USDA, 2000; USDA, 2001). Due to a variety of topographic, meteorological, and vegetative conditions, the fire created a mosaic of burn severities throughout the fire scar (Lentile et al., 2005). This mixed-severity fire resulted in 27% of the burned area classified as high severity (trees devoid of needles), 48% moderate severity (crowns entirely or almost entirely scorched), and 25% low severity (trees all or partially green) (Gould, 2003). Like many recent fires in ponderosa pine forests, the Jasper fire was initially perceived as dominated by stand-replacing components, however, Lentile et al. (2005) documented many small patches of high severity fire interspersed in a matrix of less severely burned forests. Land management activities, including salvage logging and cattle grazing, occurred in many burned locations within the first growing season following the Jasper fire.
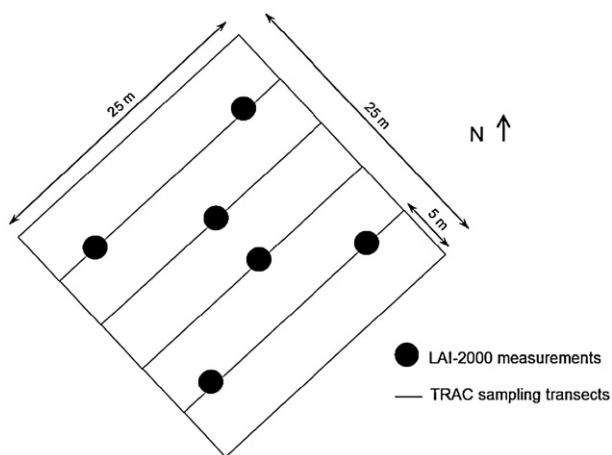

Fig. 1. Layout of six TRAC sampling transects and six LAI-measurement points within a 25 × 25 m field sampling plot.

Table 1
Leaf area index (LAI) ground sampling and Landsat and MISR image acquisition dates

Time period	LAI sampling dates	Landsat image date	MISR image date	MISR sun zenith angle	[a]No. sites	[b]No. plots
2002-1	July 7–16	July 2	July 2	23–26	13	58
2002-2	July 22–29	Aug 10	Aug 3	29–31	13	61
2002-3	Aug 21–Sept 1	Aug 19	Aug 19	32–35	11	48
2003-1	June 17–23	June 11	July 12	24–26	9	39
2003-2	July 19–21	July 20	July 21	26–29	9	42
2003-3	Aug 20–22	Aug 14	Aug 22	34–36	9	40

[a]Sampling sites are 250 m × 250 m areas having the same burn severity.
[b]Sampling plots are located within each site and are ~ 25 m × 25 m or equivalent to one Landsat pixel.

2.2. LAI ground measurements

We established fourteen sites for field data collection throughout the Jasper fire and surrounding area in spring of 2002. Three post-fire severity classes and unburned control sites were used to collect LAI measurements: high severity (5 sites), moderate severity (3 sites), low severity (3 sites) and unburned (3 sites). Sites were at least 250 m × 250 m, located on relatively flat terrain (slope < 5%), and comprised of homogeneous burn severity and vegetation species. Three to eight 25 × 25 m sampling plots were located within each of the 14 sites. In six of the sites, four of the plots were grouped together as a 50 × 50 m 'superplot' in order to address scaling questions in a related study. All plots were geographically referenced using differential GPS so that plot corners were all oriented in the four cardinal directions. Six sampling transects were established within each 25 × 25 m plot and oriented in a SE–NW direction to reduce the influence of shadow from the operator during optical data acquisition in the field (Fig. 1). LAI measurements were made during six sampling periods from June to August in 2002 and 2003, in 40 to 61 sampling plots within 9 to 13 sites (Table 1).

LAI was calculated using the following equation (Chen, 1996; Chen et al., 1997):

$$\text{LAI} = (1-\alpha)L_e\gamma_E/\Omega_E \tag{1}$$

where L_e is effective LAI, γ_E is needle-to-shoot area ratio, Ω_E is a factor describing foliage clumping for scales larger than the shoot, and α is the woody-to-total area ratio ($\alpha = W/(L_e(\gamma_E/\Omega_E))$). W represents the wood surface area index (half the total wood surface m^{-2} ground), including the contribution of branches and stems. For W and γ_E, we used values previously published for ponderosa pine; $W = 0.27$ (Law et al., 2001b) and $\gamma_E = 1.25$ (Law et al., 2001a). Ω_E was calculated using data from a Tracing Radiation and Architecture of Canopies instrument (TRAC, 3rd Wave Engineering, Ontario, Canada; Chen & Cihlar, 1995). TRAC data were collected under bright and clear sky conditions, using a walking pace of 1 m per 3 s and an instrument sampling frequency of 32 Hz resulting in a TRAC measurement interval of approximately 10 mm. The Ω_E values for each of the six transects were averaged for each plot (mean = 0.83, standard error = 0.01). L_e was measured with a LAI-2000 instrument (Li-COR, Lincoln NE) at six locations distributed systematically within

each 25×25 m plot (Fig. 1). LAI-2000 measurements were taken consecutively from both the ground level (total L_e) and above the understory vegetation (canopy L_e). LAI-2000 measurements were acquired during dusk or under overcast skies, i.e. under predominantly diffuse irradiance conditions. Reference and field measurements with the LAI-2000 instruments were taken quasi-simultaneously. Total and canopy LAI measurements were averaged across each plot prior to analysis.

2.3. LAI modeling and mapping

To enable comparisons between 1.1 km spatial resolution MISR data and LAI ground data, we used a vegetation index calculated from Landsat imagery to empirically model ground LAI continuously across a broader region encompassing our study sites. Empirical modeling approaches are commonly used to scale-up ground LAI measurements for comparison with data from a coarse resolution sensor (Cohen et al., 2003b; Wang et al., 2004; X. Chen et al., 2005c). Landsat data were acquired on six dates corresponding as closely as possible to ground data collection (Table 1). Landsat 7 ETM+ data were used in 2002 and Landsat 5 TM in 2003. Both have a spatial resolution of 30 m. A GIS road feature map was used to determine that the August 10, 2002 Landsat ETM+ image contained the highest level of geometric accuracy. The August 2002 image was also cloud-free and was therefore used as the base image for georegistration and normalization purposes. Each Landsat data set was converted to at-satellite reflectance and corrected for atmospheric effects using a simple Dark Object Subtraction method. A temporally invariant cluster method (X. Chen et al., 2005b) was used to normalize all data to the August 2002 base image. When clouds and their shadows were present, we masked and excluded these pixels from analysis.

To model LAI, we used the reduced simple ratio (RSR), which is a vegetation index calculated from red ($\rho\lambda_{red}$), near-infrared ($\rho\lambda_{NIR}$), and shortwave infrared reflectance ($\rho\lambda_{SWIR}$) (Brown et al., 2000), where

$$\text{RSR} = \frac{\rho(\gamma_{NIR})}{\rho(\gamma_{red})} \left[1 - \frac{\rho(\lambda_{SWIR}) - \rho(\lambda_{SWIRmin})}{\rho(\lambda_{SWIRmax}) - \rho(\lambda_{SWIRmin})} \right] \qquad (2)$$

and where $\rho(\lambda_{SWIRmin})$ and $\rho(\lambda_{SWIRmax})$ are the 1% minimum and maximum reflectance in Landsat SWIR band 5 within each image (Brown et al., 2000; Chen et al., 2002). The RSR has been shown to be strongly correlated with LAI in conifer forests (Chen et al., 2002; X. Chen et al., 2005c).

We fit statistical models of total and canopy LAI using both traditional regression and a non-parametric regression method. The non-parametric Theil–Sen regression does not assume a normal distribution, is robust to outliers (Theil, 1950), and has been promoted for use when measurement errors are present (Fernandes & Leblanc, 2005).

The traditional regression models were fit using the linear mixed-effects (lme) and generalized least squares (gls) model functions of the open-source statistical language R (Pinheiro & Bates, 2000; R Development Core Team, 2005). Mixed-effects models include random effects that can account for correlated error among observations. In this case, residuals from plots in

the same sampling site and/or superplot may be correlated. We included random effects in order to achieve the best and most appropriate model fits, but we used only the fixed effect from these models for LAI prediction and to calculate error statistics. The lme and gls functions allowed us to remove heteroscedasticity in residuals by using weighted variance functions (Pinheiro & Bates, 2000), which was preferable to applying transformations to the LAI response variables. We fit models of total and canopy LAI for each of the six sampling periods, in which RSR was the only fixed effect. For each of these 12 models, we fit models having three different levels of random effects: no random effects (using gls), sampling site, or sampling site and superplot. For LAI prediction we used the model structure having the lowest Akaike's information criterion (AIC) and root mean squared error (RMSE). AIC is a measure of model fit that is equivalent to the log likelihood penalized for the number of parameters (Burham & Anderson, 1998). RMSE is the standard deviation (SD) of the fitted values, expressed in units of LAI, and based upon only the fixed effect, RSR. If heteroscedasticity was present in residuals, we applied weighted variance functions. We calculated an R^2 analog (R^2_{an}) as a measure of model fit for the full model including the random effects. R^2_{an} is equal to the variance of the response variable minus the variance of the residuals corresponding to the full model, divided by variance of the response variable. We summarized error in the models using RMSE and bias. Bias is the difference between predicted and observed values of LAI. We also calculated a variance ratio, which is the SD of the predicted values divided by the SD of the observed values and represents the degree of variance compression (Cohen et al., 2003a). A variance ratio of less than one means that the predicted variance was less than the observed variance.

We fit the Theil–Sen regression models in the median based-linear models (mblm) R package using the Seigel repeated medians approach, which is robust to 50% of outliers (Siegel, 1982; Theil, 1950). The regression formulas were equivalent to those used in the gls models, and we calculated RMSE, R^2_{an}, bias, and variance ratio as described previously.

For each of the sampling periods, we applied our statistical models of LAI across Landsat-derived RSR images, using the coefficients in Table 2. Negative LAI values resulting from the models were constrained to zero. We resampled the resulting LAI images to a spatial resolution of 1.1 km using the ENVI

Table 2
Model coefficients for prediction of leaf area index (LAI) from Landsat reduced simple ratio (RSR), using generalized least squares or linear mixed-effects models

Time period	Total LAI	Canopy LAI
2002-1	$0.43 + 0.31(\text{RSR})$[a/c]	$-0.25 + 0.34(\text{RSR})$[a]
2002-2	$0.27 + 0.42(\text{RSR})$[b]	$-0.45 + 0.50(\text{RSR})$[c]
2002-3	$0.02 + 0.43(\text{RSR})$[a]	$-0.42 + 0.44(\text{RSR})$[a]
2003-1	$0.60 + 0.35(\text{RSR})$	$-0.48 + 0.39(\text{RSR})$
2003-2	$0.18 + 0.35(\text{RSR})$[c]	$-0.40 + 0.30(\text{RSR})$[b/c]
2003-3	$-0.45 + 0.59(\text{RSR})$[b/c]	$-1.15 + 0.69(\text{RSR})$[b]

[a] Full model included sampling site as a random effect.
[b] Full model included sampling site and superplot as nested random effects.
[c] Weighted variance functions were applied to remove heteroscedasticity.

pixel aggregate function, which averaged values from all contributing 30 m pixels. We expanded our study area to include unburned forest to the east of the Jasper fire area, for a total extent of 651 km^2. This allowed us to include a larger number of sampling points in our analysis and to better represent the upper range of LAI values in the Black Hills, because the majority of the area within the Jasper fire extent where ground sampling sites were located had burned.

2.4. MISR data

MISR level 2 land surface parameters (version 0017) were acquired on six dates corresponding as closely as possible with LAI ground sampling dates (Table 1). The MISR sensor records each of four spectral bands (blue, green, red, NIR) at nine view angles (±70.5°, ±60°, ±45.6°, ±26.1°, and 0° from nadir) (Diner et al., 1998). MISR level 2 surface parameters have a 1.1 km spatial resolution. Mean geolocation error is below 50 m for eight of the nine cameras, with standard deviations ranging from 60 to 100 m. The camera at 70.5° from nadir has a geolocation error below 150 m (Data Quality Statement, 10 March 2004, http://eosweb.larc.nasa.gov/PRODOCS /misr/ Quality_ Summaries). We used a MISR extension (NASA Langley Atmospheric Sciences Data Center, Hampton, VA) for ENVI image processing software (Research Systems Incorporated, Boulder, CO) to access the MISR data and associated geographic coordinates, and we converted the geographic projection to that of the Landsat imagery (UTM Zone 13 N, datum NAD27, spheroid Clarke 1866).

We used two MISR level 2 parameters, the BRF and the LAI product. The BRF is the ratio of the radiance leaving the surface to that reflected by a Lambertian surface illuminated in a single direction, in the absence of atmospheric effects (Martonchik et al., 1998). MISR LAI in conifer forest is defined as the projected needle leaf area per unit ground area, and because the contribution of the understory vegetation and soil are removed (Knyazikhin et al., 1998b), it is equivalent to our ground measurements of canopy LAI. The BRF data were Stage 1 validated, and the LAI product had provisional status.

We calculated the NDVI and the enhanced vegetation index (EVI) using BRF data from each of the nine MISR view angles. NDVI is a commonly used index calculated from red and near-infrared (NIR) reflectance (Rouse et al., 1974):

$$NDVI_\theta = \frac{\rho(\lambda_{NIR\theta}) - \rho(\lambda_{red\theta})}{\rho(\lambda_{NIR\theta}) + \rho(\lambda_{red\theta})} \tag{3}$$

EVI is less sensitive to soil and atmospheric effects than NDVI and is calculated using blue, red, and NIR reflectance (Huete et al., 2002; Miura et al., 2001), so that

$$EVI_\theta = G \frac{\rho(\lambda_{NIR\theta}) - \rho(\lambda_{red\theta})}{\rho(\lambda_{NIR\theta}) + C_1\rho(\lambda_{red\theta}) - C_2\rho(\lambda_{blue\theta})} \tag{4}$$

where G is a gain factor for the entire equation, C_1 and C_2 are adjustment factors for aerosol influences, and L is a soil adjustment factor based on the nonlinear extinction of red and NIR wavelengths through the canopy (Huete et al., 1997). We

used parameters suggested by Huete et al. (1997), where $G = 2.5$, $C_1 = 6$, $C_2 = 7.5$, and $L = 1$.

We calculated two previously published and two new anisotropic indices that incorporated the reflectance "hot spot" and "dark spot". The hot spot is the maximum reflectance that occurs in the backscatter direction when the sensor view angle and sun zenith angle are the same, while the dark spot occurs in the location with minimum reflectance in the forward scattering direction (Hapke et al., 1996; Lacaze et al., 2002; Sandmeier et al., 1998). For the hot spot, we used the BRF from the backscatter view angle closest to the sun zenith angles (−26.1°) (Table 1). We calculated the normalized difference anisotrophic index (NDAX) (Sandmeier & Deering, 1999b) from BRF anisotropy index (ANIX) data:

$$NADX = \frac{ANIX_{red} - ANIX_{NIR}}{ANIX_{red} + ANIX_{NIR}} \tag{5}$$

where ANIX represents the ratio of the hot spot and dark spot BRF for a spectral band (Sandmeier et al., 1998). We calculated the Hotspot–DarkSpot Index (HDS) (Lacaze et al., 2002) from the hot spot (HS) and dark spot (DS) of the red BRF, where

$$HDS = \frac{HS_{red} - DS_{red}}{DS_{red}} \tag{6}$$

We also calculated a new Hotspot–Darkspot NDVI (NDVI$_{HD}$) in order to maximize the contrast between red and NIR reflectance, so that

$$NDVI_{HD} = \frac{HS_{NIR} - DS_{red}}{HS_{NIR} + DS_{red}} \tag{7}$$

and, finally, we adjusted at-nadir NDVI to incorporate the hot spot from the red BRF:

$$NDVI_{HS} = NDVI_{(nadir)}(1 - HS_{red}) \tag{8}$$

2.5. LAI-MISR data analysis

We randomly generated 200 points, at least 1.1 km apart, within our 651 km^2 study area. Points having a slope greater than 4% were then eliminated to reduce interference due to complex terrain, resulting in 145 points. We extracted data from the Landsat LAI and MISR BRF and LAI pixels corresponding to these 145 geographic locations. In order to compare data from the same locations over time, we eliminated any points that had missing data for at least one sampling period, resulting in 71 and 42 data points for the analyses including MISR BRF and LAI data, respectively. All 42 points used for the LAI product comparison had a quality estimate of the highest level (QA = 0).

We fit simple linear regressions with total or canopy LAI as the response variables and NDVI or EVI, calculated from each MISR view angle, as the predictor variables, using the lm function of R (R Development Core Team, 2005). We also fit regressions with total or canopy LAI as the response variables and either NDVI$_{HD}$ or NDVI$_{HS}$ as predictor variables. We fit additional models of LAI that included NDVI at-nadir as the first term and NADX or HDS as the second term. To determine whether NADX or HDS

explained variation in LAI beyond that explained by NDVI, we used F tests from a sequential ANOVA to test for statistical significance at $\alpha = 0.05$. Finally, we fit regressions with our mapped canopy LAI as the response variable and MISR LAI as the predictor variable. We accounted for larger uncertainties in our Landsat-derived canopy LAI relative to MISR LAI (Tan et al., 2005) by binning the Landsat-derived canopy LAI values to a precision of 0.1, corresponding to their standard error (Table 3), prior to model fitting. All models were fit for each sampling period. For all models, residual and quantile–quantile plots were assessed, and Box–Cox tests were used to determine whether data transformations were suggested. When they improved diagnostic plots of residuals, transformations were applied. We compared model fits using adjusted R^2.

3. Results

3.1. LAI modeling and mapping

Models fit with traditional regression methods, on average, had higher R^2_{an} (0.72 vs. 0.46) and lower RMSE (0.45 vs. 0.55) than Theil–Sen regression models (Tables 3 and 4). The average variance ratio was higher for Theil–Sen than traditional re-

Table 3
Model fit and error statistics for generalized least squares and linear mixed-effects models predicting leaf area index (LAI) from the Landsat reduced simple ratio (RSR)

Time period	R^2_{an} [a]	RMSE[b]	Variance ratio	Measured LAI	Predicted LAI	Bias
Total LAI						
2002-1	0.86	0.28	0.34	1.51, 0.12 (0.03,3.44)	1.46, 0.11 (0.95,1.95)	−0.04 (−1.90,1.13)
2002-2	0.92	0.45	0.68	1.32, 0.09 (0.19,2.64)	1.29, 0.07 (0.68,2.46)	−0.04 (−1.22,0.76)
2002-3	0.82	0.48	0.77	1.04, 0.09 (0.01,2.29)	1.05, 0.08 (0.48,1.87)	0.00 (−0.76,0.78)
2003-1	0.23	0.35	0.47	2.08, 0.12 (0.54,4.17)	2.08, 0.06 (1.38,2.58)	0.00 (−1.64,1.39)
2003-2	0.45	0.50	0.69	1.98, 0.11 (0.46,3.62)	1.98, 0.08 (0.96,3.01)	0.00 (−1.46,1.03)
2003-3	0.98	0.56	0.78	1.44, 0.11 (0.24,2.67)	1.38, 0.11 (0.44,2.20)	−0.07 (−1.02,0.65)
Canopy LAI						
2002-1	0.85	0.30	0.34	0.90, 0.12 (0.00,3.08)	0.88, 0.10 (0.33,1.42)	−0.02 (−2.13,1.33)
2002-2	0.53	0.54	0.75	0.76, 0.09 (0.00,2.23)	0.76, 0.07 (0.04,2.15)	0.00 (−1.25,1.05)
2002-3	0.93	0.50	0.72	0.62, 0.10 (0.00,2.17)	0.64, 0.09 (0.05,1.48)	0.02 (−0.75,0.68)
2003-1	0.25	0.39	0.50	1.14, 0.12 (0.00,2.72)	1.14, 0.06 (0.37,1.68)	0.00 (−1.74,1.29)
2003-2	0.86	0.43	0.49	1.17, 0.13 (0.00,3.34)	1.13, 0.11 (0.26,2.02)	0.04 (−2.05,1.29)
2003-3	0.94	0.66	0.84	0.99, 0.12 (0.00,2.36)	0.99, 0.11 (−0.11,1.95)	−0.01 (−0.91,0.58)

For measured and predicted LAI means are followed standard error, with minimum and maximum values in parentheses. For bias, means are followed by minimum and maximum values in parentheses.
[a] R^2_{an} is an R^2 analog based on the full model (see text for details).
[b] Root mean square error (RMSE) is the standard deviation of the predicted values of LAI.

Table 4
Model fit and error statistics for Theil–Sen regression models predicting leaf area index (LAI) from the Landsat reduced simple ratio (RSR)

Time period	R^2_{an} [a]	RMSE[b]	Variance ratio	Measured LAI	Predicted LAI	Bias
Total LAI						
2002-1	0.50	0.68	0.73	1.51, 0.12 (0.03,3.44)	1.68, 0.09 (0.42,2.89)	0.17 (−1.61,1.49)
2002-2	0.49	0.51	0.77	1.32, 0.09 (0.19,2.64)	1.34, 0.07 (0.65,2.66)	0.01 (−1.16,0.83)
2002-3	0.58	0.61	0.98	1.04, 0.09 (0.01,2.29)	1.15, 0.09 (0.43,2.18)	0.10 (−0.73,1.09)
2003-1	0.21	0.26	0.35	2.08, 0.12 (0.54,4.17)	2.21, 0.04 (1.69,2.58)	0.13 (−1.63,1.47)
2003-2	0.41	0.62	0.85	1.98, 0.11 (0.46,3.62)	2.09, 0.11 (0.83,3.38)	0.11 (−1.30,1.07)
2003-3	0.70	0.68	0.95	1.44, 0.11 (0.24,2.67)	1.46, 0.11 (0.31,2.47)	0.02 (−0.96,0.79)
Canopy LAI						
2002-1	0.36	0.51	0.57	0.90, 0.12 (0.00,3.08)	0.84, 0.07 (−0.09,1.74)	−0.06 (−2.13,1.59)
2002-2	0.53	0.49	0.69	0.76, 0.09 (0.00,2.23)	0.60, 0.06 (−0.05,1.88)	−0.15 (−1.42,0.87)
2002-3	0.41	0.41	0.59	0.62, 0.10 (0.00,2.17)	0.28, 0.06 (−0.20,0.97)	−0.34 (−1.23,0.17)
2003-1	0.24	0.33	0.43	1.14, 0.12 (0.00,2.72)	1.29, 0.05 (0.63,1.75)	0.15 (−1.56,1.42)
2003-2	0.28	0.82	0.95	1.17, 0.13 (0.00,3.34)	1.06, 0.13 (−0.61,2.78)	−0.10 (−1.97,1.37)
2003-3	0.76	0.65	0.83	0.99, 0.12 (0.00,2.36)	0.93, 0.10 (−0.15,1.89)	−0.06 (−0.97,0.53)

For measured and predicted LAI means are followed standard error, with minimum and maximum values in parentheses. For bias, means are followed by minimum and maximum values in parentheses.
[a] R^2_{an} is an R^2 analog based on the full model (see text for details).
[b] Root mean square error (RMSE) is the standard deviation of the predicted values of LAI.

gression, but this improvement was small, 0.72 as compared with 0.61. Because of higher R^2_{an}, and lower RMSE and bias, we chose to use coefficients from the traditional models for our LAI predictions (Table 2).

Overall, we found strong relationships between the Landsat RSR and ground measurements of total and canopy LAI, with an average R^2_{an} of 0.72 across sampling dates (Table 3). Based on low R^2_{an} values (0.23–0.25), we eliminated data from the 2003-1 sampling period from further analyses. There was also a one month difference in acquisition dates between cloud-free Landsat and MISR data for the 2003-1 sampling period, which further supported its removal (Table 1). Mean values for LAI measured in the field and predicted from the models were generally the same. Predictions of the lowest total and canopy LAI values were consistently overestimated by the models, while predictions of the highest values were consistently underestimated (Table 3). This trend is the result of variance compression (Cohen et al., 2003a). The variance was least compressed during the late summer sampling periods and most compressed during the early summer sampling periods (Table 3). Models of total LAI had lower RMSE (relative to ranges in measured and predicted LAI values) than did models of canopy LAI. Average variance compression was the same for total and canopy LAI. Mean bias was typically zero, but the
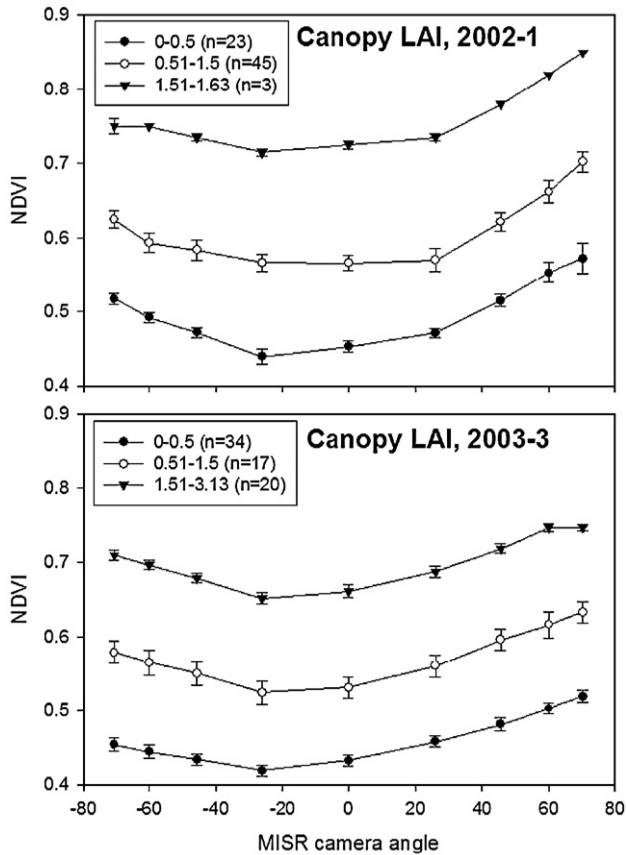
Fig. 2. MISR angular signatures of NDVI for three categories of canopy LAI, during early (2002-1) and late summer (2003-3) sampling periods. Error bars represent standard error around the mean. MISR camera angle units are in degrees.

range in bias showed that Landsat predicted values tended to underestimate ground LAI measurements (Table 3).

3.2. LAI-MISR relationships

Differences in LAI were best explained by the magnitude of NDVI, rather than by differences in the anisotropy of NDVI (Fig. 2). NDVI angular signatures exhibited a slight bowl-shape, which is to be expected from a relatively open forest canopy. The degree to which these signatures were bowl-shaped did not vary greatly among three categories of canopy LAI values (Fig. 2).

We found the best model fits for canopy and total LAI using either $NDVI_{HS}$, models including both at-nadir NDVI and either NADX or HDS, or NDVI calculated from the $-60°$ view angle (Table 5). Model fits were generally good, with adjusted R^2 values for best-fitting models ranging from 0.82 to 0.91 for all models except those corresponding to the 2002-2 sampling period, where the best-fitting models had R^2 values of 0.54 and 0.56. Model fits were nearly identical for canopy and total LAI, with a maximum difference in R^2 of 0.02 between the best-fitting models for each type of LAI. The differences between the adjusted R^2 values for the best-fitting models and those including only at-nadir NDVI were small, ranging from 0.01 to 0.08 (Table 5). In the models including both at-nadir NDVI

and either HDS or NADX, NDVI was always highly statistically significant ($p < 0.001$). In most cases, the inclusion of HDS or NADX did not explain additional variation in LAI beyond that explained by NDVI. The exceptions were that during the 2003-3 sampling period HDS and NADX explained additional variation in both canopy and total LAI, and the same was true for total LAI for the 2002-1 sampling period (Table 6). The statistical significance of HDS and NADX did not greatly affect model fit, although these were the best-fitting models for total LAI in 2002-1 and 2003-3.

Models with NDVI and off-nadir or anisotropic versions of NDVI generally had higher R^2 values than those with EVI or off-nadir EVI. Model fits for NDVI and EVI calculated across

Table 5
Adjusted R^2 values for linear regression models of canopy and total LAI predicted from NDVI, EVI and anisotropic indices

	2002-1	2002-2	2002-3	2003-2	2003-3
Canopy LAI					
NDVI (nadir)	0.83	0.48	0.82	0.79	0.85
NDVI (off-nadir)[a]	NA	0.54[e]	**0.83**[d]	NA	0.88[e]
EVI (nadir)	0.81	0.41	0.80	0.69	0.81
EVI (off-nadir)[a]	NA	0.46[e]	0.81[d]	0.71[b]	0.85[e]
NDVI+NADX	0.83	0.54	**0.83**	0.83	0.87
NDVI+HDS	**0.84**	0.54	0.82	0.79	0.86
$NDVI_{HD}$	0.77	0.16	0.79	0.65	0.86
$NDVI_{HS}$	0.82	**0.56**	0.82	0.84	**0.89**
Total LAI					
NDVI (nadir)	0.83	0.50	0.79	0.84	0.89
NDVI (off-nadir)[a]	NA	**0.54**[e]	0.80[d]	NA	**0.91**[e]
EVI (nadir)	0.82	0.37	0.78	0.71	0.86
EVI (off-nadir)[a]	NA	0.47[e]	NA	0.72[c]	0.89[e]
NDVI+NADX	0.83	0.53	**0.82**	0.84	**0.91**
NDVI+HDS	**0.84**	0.53	0.81	0.84	0.90
$NDVI_{HD}$	0.77	0.18	0.76	0.67	0.88
$NDVI_{HS}$	0.83	0.53	0.81	**0.85**	0.89

The highest R^2 value for each sampling period and LAI type is shown in bold.
[a] R^2 value from the off-nadir index is reported if it higher than that of the model using the index at-nadir.
[b–e] The off-nadir index that improved model fit was calculated from the following MISR view angles: $b = -26.1°$, $c = -45.6°$, $d = -60°$, and $e = -70.5°$.

Table 6
Sequential ANOVA p-values from models of canopy and total LAI in which NDVI was the first term and HDS or NDAX the second

	HDS	NADX
Canopy LAI		
2002-1	0.08	0.07
2002-2	0.41	0.53
2002-3	0.49	0.06
2003-2	0.40	0.43
2003-3	**<0.01**	**<0.01**
Total LAI		
2002-1	**0.03**	**0.03**
2002-2	0.40	0.53
2002-3	0.61	0.14
2003-2	0.45	0.33
2003-3	**0.01**	**<0.01**

Statistically significant p-values ($\alpha = 0.05$) are shown in bold. The first term, NDVI, was statistically significant in all models ($p < 0.001$).
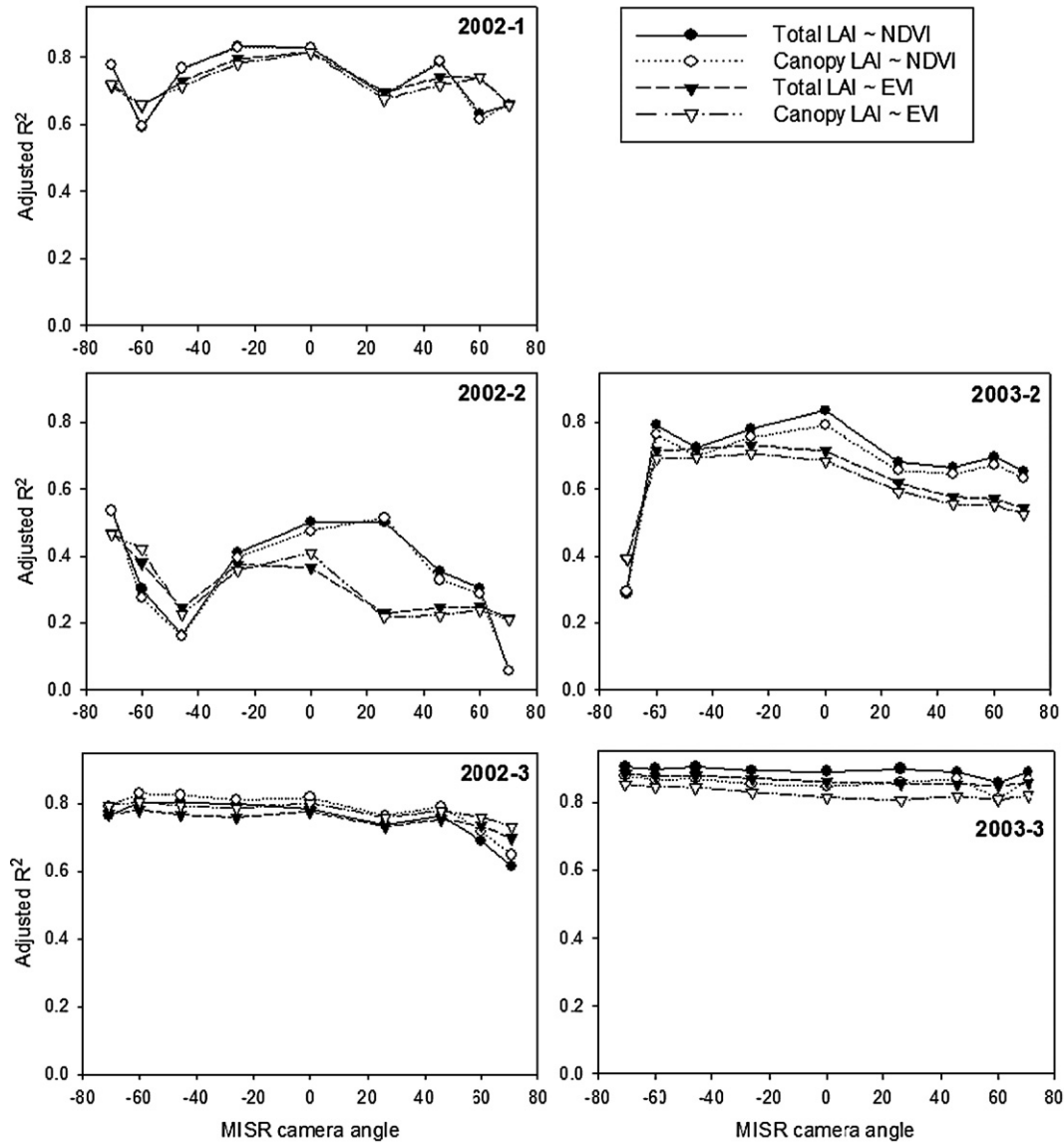
Fig. 3. Adjusted R^2 values from simple linear models of canopy or total LAI, with NDVI or EVI calculated at each MISR view angle as predictor variables.

all MISR view angles showed much more variation during the earlier summer sampling periods than during the later summer sampling periods (Fig. 3). This pattern was the same for canopy and total LAI.

We found relatively poor fits between the MISR LAI product and our Landsat-derived estimates of canopy LAI, with adjusted R^2 values ranging from 0.21 to 0.44 (Fig. 4). The relationship between our LAI estimates and the MISR LAI was close to the 1:1 line in the 2002-2, 2003-2 and 2003-3 sampling periods, but our Landsat-derived LAI was overestimated by the MISR LAI product in the 2002-1 and 2002-3 sampling periods (Fig. 4).

4. Discussion and conclusions

4.1. LAI modeling and mapping

The 10 gls and lme linear regression models that we used to predict LAI surfaces had an average R^2_{an} of 0.81. The models

also had low RMSE (0.3–0.7, in LAI units) and only negligible negative bias (Table 3). A trade-off of these good fits and low error was that the variance of the predicted LAI only retained 34 to 84% of the variance present in the measured LAI values. Variance compression has been reduced or eliminated in previous studies through the use of regression methods that correctly assume there is error in both predictor and response variables (Cohen et al., 2003a,b). Errors from field measurements and the Landsat data used to extrapolate them across a landscape can reduce precision of LAI estimates (Tan et al., 2005). Although we fit Theil–Sen regression models, which account for such measurement errors, we did not find that it decreased variance compression enough to justify higher error. We might have found even less variance compression had we applied reduced major axis, or geometric mean regression (GMA), a method with similar assumptions to Theil–Sen regression (Cohen et al., 2003a), but GMA has been found to result in higher RMSE than either traditional or Theil–Sen
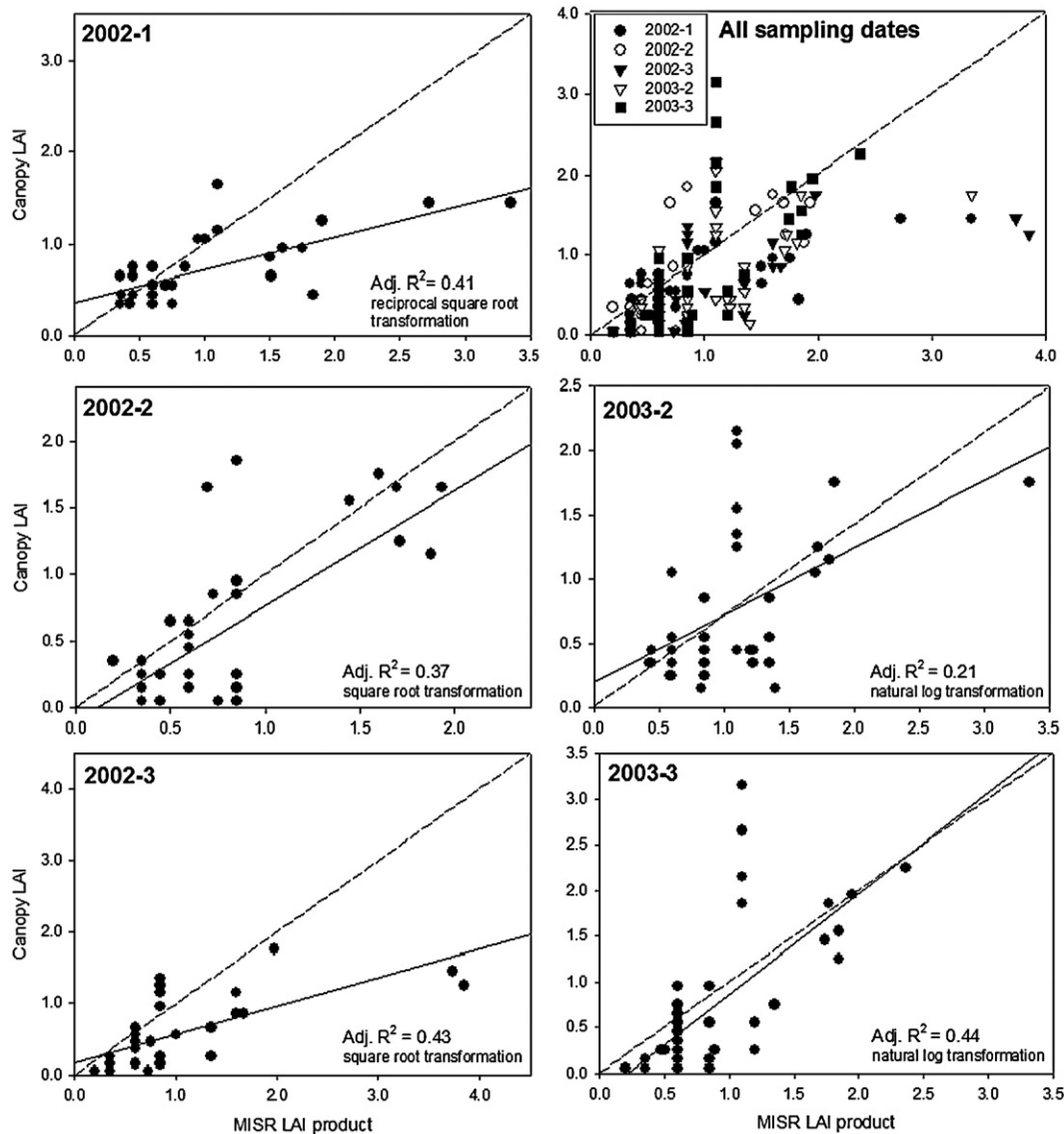
Fig. 4. Comparison between the MISR LAI product and Landsat-derived, ground-based measurements of canopy LAI, at 42 points. Each plot represents a different sampling period. Linear regression lines are solid and 1:1 lines are dotted.

regression (Fernandes & Leblanc, 2005). In our case low error appeared preferable to a preserved variance structure. Preservation of LAI variance would have been given preference had our purpose been to use our predicted LAI surfaces as part of mechanistic models (Cohen et al., 2003a).

We found less error in models of total LAI than in those of canopy LAI (Table 3). It is to be expected that total LAI or greenness would have a stronger correlation with the Landsat RSR than just a portion of that greenness. We also found the best model fits and least variance compression during the late summer sampling period, when the contribution of the understory vegetation to the reflectance signal would be lowest. The pattern of reduced variance compression with improved model fit has been noted previously (Cohen et al., 2003b). We report errors at the scale of 30 m Landsat pixels, but the aggregation of 1225 Landsat pixels to the 1.1 km MISR spatial resolution may have reduced our reported LAI RMSE (Fernandes et al., 2003).

4.2. LAI-MISR relationships

We found improved model fits for both canopy and total LAI when we used NDVI calculated from off-nadir view angles or included anisotropic indices in our models in addition to at-nadir NDVI. However, these 1 to 8% improvements in adjusted R^2 may not represent statistically significant differences. The inclusion of HDS or NADX in models of LAI explained significant variation in LAI (beyond that explained by NDVI) in only a few cases (Table 6) and without large improvements in adjusted R^2 (Table 5). HDS calculated from POLDER data has been previously correlated with foliage clumping at a coarse spatial resolution (7 km), but across more diverse vegetation types (Chen et al., 2003). NADX has previously explained variation related to tree species and canopy shapes, but at a much finer spatial resolution of 3.7 m (Sandmeier & Deering, 1999b). Although these indices were correlated with different canopy attributes in past studies, they appeared to explain the

same variation in our study area. We may have found only small improvements using data from multiple view angles because our study area is dominated by a single tree species, ponderosa pine, in open stands typically having less than 70% canopy cover. The BRF of forests has been largely explained by differences in tree species, crown shapes (Lobell et al., 2002; Rautiainen et al., 2004; Sandmeier & Deering, 1999a), and forest stand density or overall canopy heterogeneity (Johnson, 1994; Nolin, 2004; Pinty et al., 2002). Greater improvements in LAI estimation using multiple view angles may occur in forest types having more diversity in tree species and stand densities. However, more diverse forests may also occur in areas with more complex terrain, which could complicate the detection of anisotropy effects. Although low LAI values allowed us to avoid NDVI saturation, a forest with higher LAI values may show a greater response to multiple view angles precisely because of this saturation effect at-nadir. Conversely, angular effects have also been found to decrease with increases in leaf area (Kaufmann et al., 2000). Kaufmann et al. (2000) found that advanced very high resolution radiometer (AVHRR) NDVI was sensitive to changes in solar zenith angles only in shrub and grassland biome types having low leaf area and sparse canopies.

The reflectance anisotropy associated with this ponderosa pine forest appeared to relate strongly to understory vegetation phenology. We found that the relationships between NDVI or EVI and LAI showed very little variation across view angles during the late summer sampling periods when the understory vegetation would have been senesced and understory LAI was lowest, while we found the most variation in this relationship during the earliest summer sampling season, when understory green LAI was greatest (Fig. 3). Despite the apparent influence of the understory vegetation, we found little or no divergence in patterns between canopy and total LAI. This could be because understory LAI showed little variation across the study area.

The bowl-shape we observed in angular signatures of NDVI may be due to the presence of relatively open forest canopies that generate many shadows (Pinty et al., 2002). This pattern may also be in response to the amount of canopy greenness, with off-nadir angles viewing more leaf material, especially when tree canopy LAI is higher than understory LAI. Angular signatures for EVI generally declined from the backscatter to forward scatter direction or were flat, likely because EVI is more sensitive to shadowing than is NDVI (X. Chen et al., 2005b). NDVI performed better than EVI in predicting LAI, especially during July sampling periods (Table 5, Fig. 3). X. Chen et al. (2005b) also found stronger correlations between NDVI and LAI than between EVI and LAI, in mixed conifer and deciduous forest. This was attributed to a "cancellation effect" that occurred because EVI was positively correlated with understory vegetation greenness but negatively correlated with forest canopy greenness when the forest shadowed green understory (X. Chen et al., 2004, 2005b). EVI has also shown a stronger correlation with the grass fraction of multispectral IKONOS imagery than has NDVI, in previous research conducted near our Black Hills study area (Chen et al., 2004). This greater sensitivity of EVI to green understory vegetation may explain why NDVI and EVI produced nearly identical

model fits of LAI during the late August summer sampling periods (Fig. 3), when the understory vegetation was senesced.

We found much lower model fits for LAI during the 2002-2 sampling period than during the other sampling periods. This does not appear to be a result of error propagation due to the modeling of ground LAI using Landsat imagery, as the model fits and error for this time period are comparable to those for the other sampling periods we assessed (Table 3). The poor model fits may be a result of rapidly changing vegetation greenness during this time period in late July and differences of as much as a week among ground data collection, Landsat image acquisition, and MISR image acquisition. We may have observed this pattern in 2002 and not during the same time period in 2003 because of differences in precipitation, temperature, and phenological pattern between the 2 years. In 2003, the understory vegetation appeared to senesce earlier than in 2002. Drier conditions during 2003 are supported by precipitation data; the nearest climate station in Custer, South Dakota received 43.5 mm of precipitation during July 2002, but only 15.3 mm during July 2003 (South Dakota Office of Climatology, http://climate.sdstate.edu/climate_site/climate.htm).

The indices we calculated from MISR BRF data explained more variation in our ground-based estimates of total LAI than did the MISR LAI product. A possible explanation for this finding is that LAI was derived in a similar manner with Landsat and MISR BRF data, using indices, while the MISR LAI product is determined using other types of algorithms.

None of the 42 points we considered in our analysis were assigned by MISR to the conifer forest biome, nor did any portion of the Black Hills, which includes large extents of unburned forest, appear to be categorized in the correct biome. Instead we found that across sampling periods, 24 (57%) of our 42 sampling points were classed as grasses and cereal crops, 7 (17%) were shrubs, 10 (24%) were missing a biome class, and 1 point was classed as broadleaf crops. This finding is consistent with incorrect biome assignment in 80% of pixels across five biomes in Africa (Hu et al., 2003). Hu et al. (2003) found minimal impact of biome misclassification on MISR LAI retrievals, so it is unlikely that biome misclassification can explain the only moderate correspondence between our Landsat-derived and MISR LAI values. MISR LAI values tended to be higher than our Landsat-derived values. We would have expected the opposite pattern if biome misclassification were responsible, because the MISR biomes assigned in our study area are characterized by lower LAI values than those typically occurring in conifer forest.

4.3. Future research needs

To our knowledge, this was the first quantitative study considering MISR view angle effects on LAI. It is encouraging that we found a small improvement in LAI estimation with off-nadir NDVI or anisotropic indices, during five separate sampling periods, using MISR BRF data despite relatively minor canopy structural variation within one forest type and MISR's coarse spatial resolution. Our findings suggest that even greater improvements in LAI estimation may be possible with multi-angle remote sensing in forested areas

including a more diverse mix of species, or at finer scale spatial resolutions.

We found that vegetation phenology was important to relationships between Landsat RSR and LAI ground data and the degree of anisotropy detected in relationships between MISR NDVI or EVI and Landsat-derived LAI. In our study area, this was largely due to contrasting greenness and senescence of understory vegetation within relatively open forest canopies between wet and dry summer sampling periods. Model fits between MISR BRF indices and LAI also appeared to be affected by how closely image and ground data acquisition dates corresponded, especially in the case of a mid-season sampling period when vegetation phenology was changing rapidly. Future research should continue to pay close attention to phenological agreement between remotely sensed and field data. To date, phenological patterns have received little attention in multi-angle remote sensing, but our findings show that the amount of knowledge gained from multiple view angles can be amplified with the consideration of multiple sampling periods. In addition, relatively few studies examine and map the variability of LAI across landscapes that have recently experienced some degree of disturbance (e.g. fire, insect outbreak). Further work to examine the ability of satellite sensors to detect LAI patterns post-disturbance will increase the utility of these measurements when monitoring ecosystems ranging in scale from a landscape to a continent.

It is impossible to avoid errors when comparing ground measurements to coarse scale remotely sensed data, because it is not yet feasible to measure LAI directly across these broader scales. However, full accounting of model error is rarely presented in studies that scale-up ground data for comparisons with coarser resolution sensors (but see Tan et al., 2005). A more consistent reporting of error measures is needed, as well as more research to understand error propagation and how to minimize its effects. Statistical methods aside from traditional linear regression should be also considered (Cohen et al., 2003a; Fernandes & Leblanc, 2005).

Acknowledgements

References

Aber, J. D., Reich, P. B., & Goulden, M. L. (1996). Extrapolating leaf CO_2 exchange to the canopy: A generalized model of forest photosynthesis compared with measurements by eddy correlation. *Oecologia, 106*, 257−265.

Asner, G. P., Braswell, B. H., Schimel, D. S., & Wessman, C. A. (1998). Ecological research needs from multiangle remote sensing data. *Remote Sensing of Environment, 63*, 155−165.

Birth, G. S., & McVey, G. (1968). Measuring the color of growing turf with a reflectance spectrophotometer. *Agronomy Journal, 60*, 640−643.

Bonan, G. B. (1993). Importance of leaf area index and forest type when estimating photosynthesis in boreal forests. *Remote Sensing of Environment, 43*, 303−314.

Brown, L., Chen, J. M., Leblanc, S. G., & Cihlar, J. (2000). A shortwave infrared modification for LAI retrieval in boreal forests: An image and model analysis. *Remote Sensing of Environment, 71*, 16−25.

Burham, K. P., & Anderson, D. R. (1998). *Model selection and inference: A practical information-theoretic approach.* New York: Springer–Verlag.

Chen, J. M. (1996). Optically-based methods for measuring seasonal variation of leaf area index in boreal conifer forests. *Agricultural and Forest Meteorology, 80*, 135−163.

Chen, J. M., & Cihlar, J. (1995). Plant canopy gap size analysis theory for improving optical measurements of leaf area index. *Applied Optics, 34*, 6211−6222.

Chen, J. M., Liu, J., Leblanc, S. G., Lacaze, R., & Roujean, J. -L. (2003). Multi-angular optical remote sensing for assessing vegetation structure and carbon absorption. *Remote Sensing of Environment, 84*, 516−525.

Chen, J. M., Pavlic, G., Brown, L., Cihlar, J., Leblanc, S. G., White, H. P., et al. (2002). Derivation and validation of Canada-wide coarse-resolution leaf area index maps using high-resolution satellite imagery and ground measurements. *Remote Sensing of Environment, 80*, 165−184.

Chen, J. M., Rich, P. M., Gower, S. T., Norman, J. M., & Plummer, S. (1997). Leaf area index of boreal forests: Theory, techniques, and measurements. *Journal of Geophysical Research, 102*, 29429−29443.

Chen, J. M., Menges, C. H., & Leblanc, S. G. (2005a). Global mapping of foliage clumping index using multi-angular satellite data. *Remote Sensing of Environment, 97*, 447−457.

Chen, X., Vierling, L., & Deering, D. (2005b). A simple and effective radiometric correction method to improve landscape change detection across sensors and across time. *Remote Sensing of Environment, 98*, 63−79.

Chen, X., Vierling, L., Deering, D., & Conley, A. (2005c). Monitoring boreal forest LAI across a Siberian burn chronosequence: A MODIS validation study. *International Journal of Remote Sensing, 26*, 5433−5451.

Chen, X., Vierling, L., Rowell, E., & DeFelice, T. (2004). Using lidar and effective LAI data to evaluate IKONOS and Landsat 7 ETM+ vegetation cover estimates in a ponderosa pine forest. *Remote Sensing of Environment, 91*, 14−26.

Cohen, W. B., Maiersperger, T. K., Gower, S. T., & Turner, D. P. (2003a). An improved strategy for regression of biophysical variables and Landsat ETM+ data. *Remote Sensing of Environment, 84*, 561−571.

Cohen, W. B., Maiersperger, T. K., Yang, Z., Gower, S. T., Turner, D. P., Ritts, W. D., et al. (2003b). Comparisons of land cover and LAI estimates derived from ETM+ and MODIS for four sites in North America: A quality assessment of 2000/2001 provisional MODIS products. *Remote Sensing of Environment, 88*, 233−255.

Deering, D. W., Eck, T. F., & Banerjee, B. (1999). Characterization of the reflectance anisotropy of three boreal forest canopies in spring–summer. *Remote Sensing of Environment, 67*, 205−229.

Deering, D. W., Middleton, E. M., & Eck, T. F. (1994). Reflectance anisotropy for a spruce–hemlock forest canopy. *Remote Sensing of Environment, 47*, 242−260.

Diner, D. J., Beckert, J. C., Reilly, T. H., Bruegge, C. J., Conel, J. E., Kahn, R. A., et al. (1998). Multi-angle imaging spectroradiometer (MISR) instrument description and experiment overview. *IEEE Transactions on Geoscience and Remote Sensing, 36*, 1072−1085.

Diner, D. J., Braswell, B. H., Davies, R., Gobron, N., Hu, J., Jin, Y., et al. (2005). The value of multiangle measurements for retrieving structurally and radiatively consistent properties of clouds, aerosols, and surfaces. *Remote Sensing of Environment, 97*, 495−518.

Fernandes, R., Butson, C., Leblanc, S., & Latifovic, R. (2003). Landsat-5 TM and Landsat-7 ETM+ based accuracy assessment of leaf area index products for Canada derived from SPOT-4 VEGETATION data. *Canadian Journal of Remote Sensing, 29*, 241−258.

Fernandes, R., & Leblanc, S. G. (2005). Parametric (modified least squares) and non-parametric (Theil–Sen) linear regressions for predicting biophysical parameters in the presence of measurement errors. *Remote Sensing of Environment, 95*, 303−316.

Gates, D. M., Keegan, H. J., Schleter, J. C., & Weidner, V. R. (1965). Spectral properties of plants. *Applied Optics, 4*, 11−20.

Gausman, H. W., Allen, W. A., Wiegand, C. L., Escobar, D. E., Rodriguez, R. R., & Richardson, A. J. (1973). The leaf mesophylls of twenty crops, their light spectra, and optical and geometrical parameters. *USDA Agric. Res. Serv. Tech. Bull.*, vol. 1465. (pp.).

Gholz, H. L. (1982). Environmental limits on above-ground net primary production, leaf area, and biomass in vegetation zones of the Pacific Northwest. *Ecology*, *63*, 469−481.

Gould, J. J. (2003) Hydrologic modeling of high-intensity, short-duration rainfall on burned ponderosa pine forested watersheds existing in highly permeable geology within the Black Hills of South Dakota. MS Thesis. South Dakota School of Mines and Technology, Rapid City, SD.

Hapke, B., DiMucci, D., Nelson, R., & Smythe, W. (1996). The cause of the hot spot in vegetation canopies and soils: Shadow-hiding versus coherent backscatter. *Remote Sensing of Environment*, *58*, 63−68.

Hu, J., Tan, B., Shabanov, N., Crean, K. A., Martonchik, J. V., Diner, D. J., et al. (2003). Performance of the MISR LAI and FPAR algorithm: A case study in Africa. *Remote Sensing of the Environment*, *88*, 324−340.

Huete, A., Dian, K., Miura, T., Rodriguez, E. P., Gao, X., & Ferreira, L. G. (2002). Overview of the radiometric and biophysical performance of the MODIS vegetation indices. *Remote Sensing of Environment*, *83*, 195−213.

Huete, A. R., Liu, H. Q., Batchily, K., & Leeuwen, V. W. (1997). A comparison of vegetation indices over a global set of TM images for EOS-MODIS. *Remote Sensing of Environment*, *59*, 440−451.

Johnson, L. F. (1994). Multiple view zenith angle observations of reflectance from ponderosa pine stands. *International Journal of Remote Sensing*, *15*, 3859−3865.

Kaufmann, R. K., Zhou, L., Knyazikhin, Y., Shabanov, N. V., Myneni, R. B., & Tucker, C. J. (2000). Effect of orbital drift and sensor changes on the time series of AVHRR vegetation index data. *IEEE Transactions on Geoscience and Remote Sensing*, *38*, 2584−2597.

Knyazikhin, Y., Martonchik, J. V., Diner, D. J., Myneni, R. B., Verstraete, M., Pinty, B., et al. (1998a). Estimation of vegetation canopy leaf area index and fraction of absorbed photosynthetically active radiation from atmosphere-corrected MISR data. *Journal of Geophysical Research*, *103*, 32239−32256.

Knyazikhin, Y., Martonchik, J. V., Myneni, R. B., Diner, D. J., & Running, S. W. (1998b). Synergistic algorithm for estimating vegetation canopy leaf area index and fraction of absorbed photosynthetically active radiation from MODIS and MISR data. *Journal of Geophysical Research*, *103*, 32257−32276.

Lacaze, R., Chen, J. M., Roujean, J. -L., & Leblanc, S. G. (2002). Retrieval of vegetation clumping index using hot spot signatures measured by POLDER instrument. *Remote Sensing of Environment*, *79*, 84−95.

Law, B. E., Cescatti, A., & Baldocchi, D. D. (2001a). Leaf area distribution and radiative transfer in open-canopy forests: Implications to mass and energy exchange. *Tree Physiology*, *21*, 777−787.

Law, B. E., Van Tuyl, S., Cescatti, A., & Baldocchi, D. D. (2001b). Estimation of leaf area index in open-canopy ponderosa pine forests at different successional stages and management regimes in Oregon. *Agricultural and Forest Meteorology*, *108*, 1−14.

Lentile, L.B. (2004) Causal factors and consequences of mixed-severity fire in Black Hills ponderosa pine forests. PhD Dissertation. Colorado State University, Fort Collins, CO.

Lentile, L. B., Smith, F. W., & Shepperd, W. D. (2005). Patch structure, fire-scar formation and tree regeneration in a large mixed-severity fire in the South Dakota Black Hills, USA. *Canadian Journal of Forest Research*, *35*, 2875−2885.

Lobell, D. B., Asner, G. P., Law, B. E., & Treuhaft, R. N. (2002). View angle effects on canopy reflectance and spectral mixture analysis of coniferous forests using AVIRIS. *International Journal of Remote Sensing*, *23*, 2247−2262.

Martonchik, J. V., Diner, D. J., Verstraete, M. M., Myneni, R. B., Knyazikhin, Y., & Gordon, H. R. (1998). Determination of land and ocean reflective, radiative, and biophysical properties using multiangle imaging. *IEEE Transactions on Geoscience and Remote Sensing*, *36*, 1266−1281.

Miura, T., Huete, A. R., Yoshioka, H., & Hoblen, B. N. (2001). An error and sensitivity analysis of atmospheric resistant vegetation indices derived from dark target-based atmospheric correction. *Remote Sensing of Environment*, *78*, 284−298.

Nemani, R., Pierce, L., Running, S., & Band, L. (1993). Forest ecosystem processes at the watershed scale: Sensitivity to remotely-sensed leaf area index estimates. *International Journal of Remote Sensing*, *14*, 2519−2534.

Nolin, A. W. (2004). Towards retrieval of forest cover density over snow from the Multi-angle Imaging SpectroRadiometer (MISR). *Hydrological Processes*, *18*, 3623−3636.

Pinheiro, J. C., & Bates, D. M. (2000). *Mixed-effects models in S and S-Plus.* New York: Springer–Verlag.

Pinty, B., Widlowski, J. -L., Gobron, N., Verstraete, M. M., & Diner, D. J. (2002). Uniqueness of multiangular measurements — Part I: An indicator of subpixel surface heterogenity from MISR. *IEEE Transactions on Geoscience and Remote Sensing*, *40*, 1560−1573.

Pocewicz, A. L., Gessler, P., & Robinson, A. R. (2004). The relationship between effective plant area index and Landsat spectral response across elevation, solar insolation, and spatial scales in a northern Idaho forest. *Canadian Journal of Forest Research*, *34*, 465−480.

Rautiainen, M., Stenberg, P., Nilson, T., & Kuusk, A. (2004). The effect of crown shape on the reflectance of coniferous stands. *Remote Sensing of Environment*, *89*, 41−52.

R Development Core Team (2005). *R: A language and environment for statistical computing. R foundation for statistical computing, Vienna, Austria.* URL: http://www.R-project.org

Rouse, J. W., Haas, R. H., Schell, J. A., & Deering, D. W. (1974). Monitoring vegetation systems in the Great Plains with ERTS. *Proceedings, Third Earth Resources Technology Satellite-1 Symposium, Greenbelt, MD. December, 1973* (pp. 301−317). Washington, DC: NASA SP-351.

Sandmeier, S., & Deering, D. W. (1999a). Structure analysis and classification of boreal forests using airborne hyperspectral BRDF data from ASAS. *Remote Sensing of Environment*, *69*, 281−295.

Sandmeier, S. R., & Deering, D. W. (1999b). A new approach to derive canopy structure information for boreal forests using spectral BRDF data. *IEEE IGARSS 1999 Proceedings* Germany: Hamburg.

Sandmeier, S., Miller, C., Hosgood, B., & Andreoli, G. (1998). Physical mechanisms in hyperspectral BRDF data of grass and watercress. *Remote Sensing of Environment*, *66*, 222−233.

Shepperd, W. D., & Battaglia, M. A. (2002). *Ecology, silviculture, and management of Black Hills ponderosa pine.* USDA Forest Service GTR-RMRS-97.

Siegel, A. F. (1982). Robust regression using repeated medians. *Biometrika*, *69*, 242−244.

Tan, B., Hu, J., Zhang, P., Huang, D., Shabanov, N., Weiss, M., et al. (2005). Validation of Moderate Resolution Imaging Spectroradiometer leaf area index product in croplands of Alpilles, France. *Journal of Geophysical Research*, *110*, 1−15.

Theil, H. (1950). A rank-invariant method of linear and polynomial regression analysis. *Netherlands Academy of Science Series A*, *53*, 386−392.

USDA Forest Service, (2000). *Jasper Fire Rapid Assessment Team Report*. USDA For. Serv. Black Hills National Forest. Supervisor's Office, 25041 North Highway 16, Custer, SD 57730.

USDA Forest Service, (2001). *Jasper Fire Value Recovery Final Environmental Impact Statement FEIS*. USDA For. Serv. Black Hills National Forest, Supervisor's Office, 25041 North Highway 16, Custer, SD 57730.

Vierling, L. A., Deering, D. W., & Eck, T. F. (1997). Differences in arctic tundra vegetation type and phenology as seen using bidirectional radiometry in the early growing season. *Remote Sensing of Environment*, *60*, 71−82.

Wang, Y., Woodcock, C. E., Buermann, W., Stenberg, P., Voipio, P., Smolander, H., et al. (2004). Evaluation of the MODIS LAI algorithm at a coniferous forest site in Finland. *Remote Sensing of Environment*, *91*, 114−127.

Waring, R. H., & Law, B. E. (2001). The ponderosa pine ecosystem and environmental stress: Past, present and future. *Tree Physiology*, *21*, 273−274.

Waring, R. H., & Running, S. W. (1998). *Forest Ecosystems: Analysis at Multiple Scales.* San Diego: Academic Press.

White, M. A., Thornton, P. E., Running, S. W., & Nemani, R. R. (2000). Parameterization and sensitivity analysis of the Biome-BGC terrestrial ecosystem model: Net Primary Production controls. *Earth Interactions*, *4*, 1−85 http://EarthInteractions.org

Widlowski, J. -L., Pinty, B., Gobron, N., Verstraete, M. M., Diner, D. J., & Davis, A. B. (2004). Canopy structure parameters derived from multi-angular remote sensing data for terrestrial carbon studies. *Climatic Change*, *67*, 403−415.